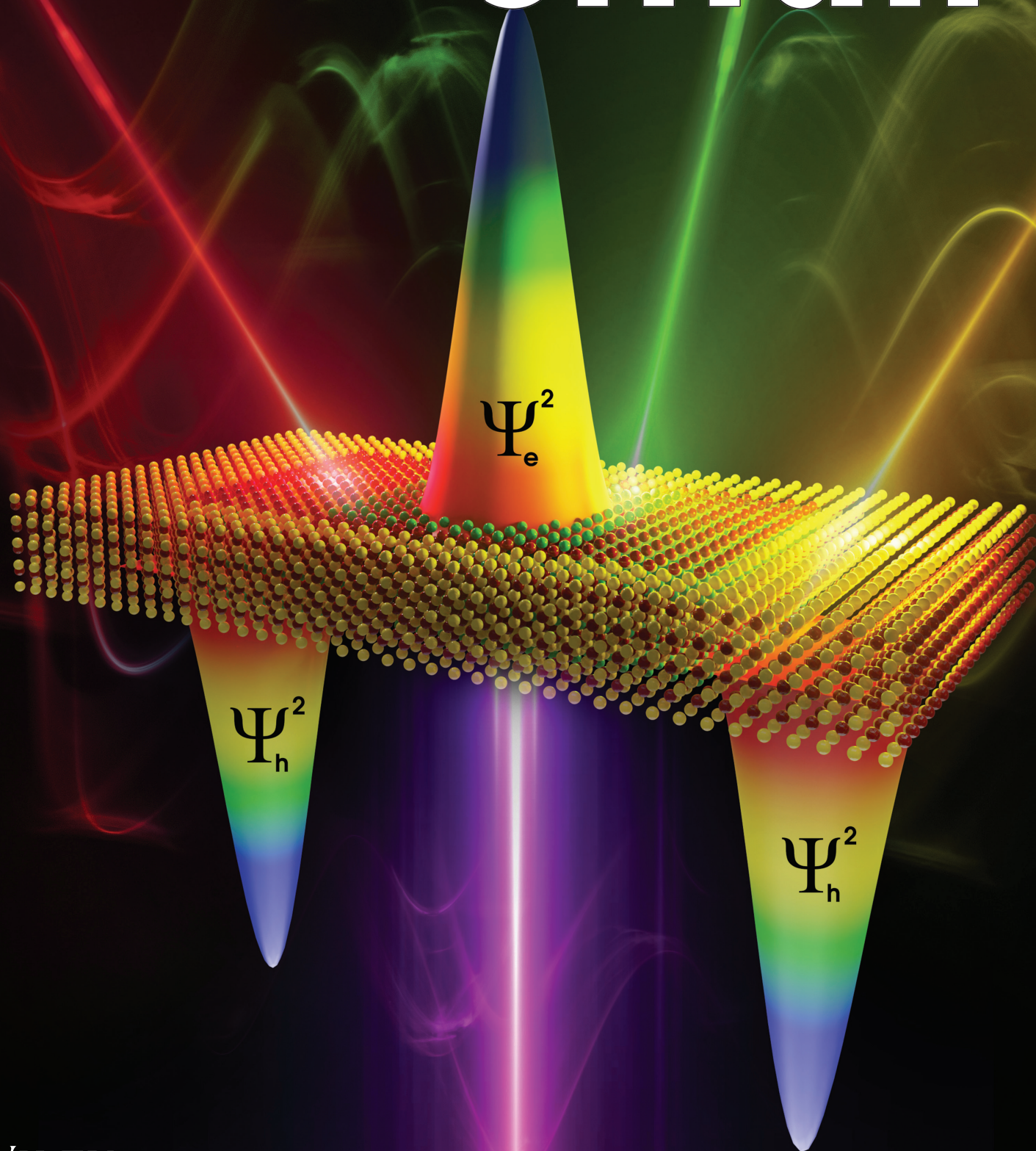


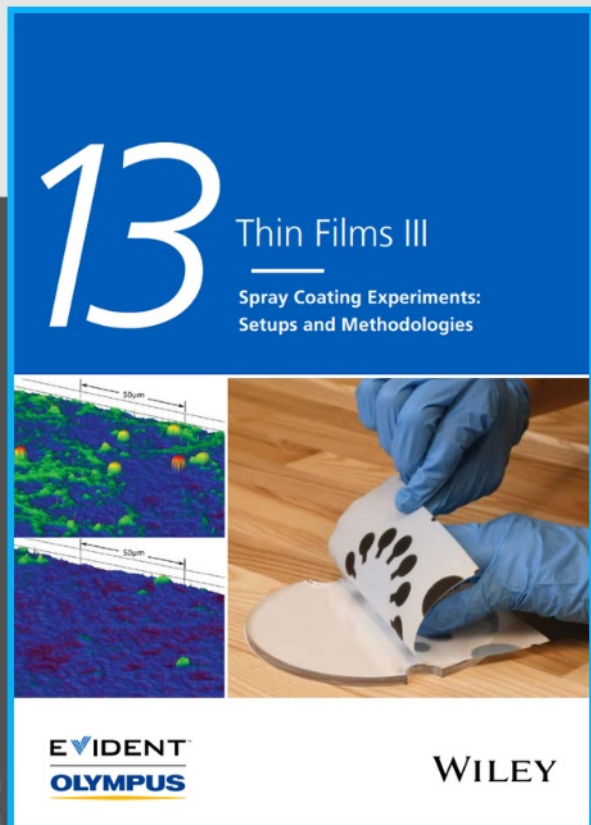
NANO • MICRO small





Spray Coating Experiments: Setups and Methodologies

**The latest eBook from
Advanced Optical Metrology.
Download for free.**



Spray Coating Experiments: Setups and Methodologies, is the third in our Thin Films eBook series. This publication provides an introduction to spray coating, three article digests from Wiley Online Library and the latest news about Evident's Image of the Year Award 2022.

Wiley in collaboration with Evident, are committed to bridging the gap between fundamental research and industrial applications in the field of optical metrology. We strive to do this by collecting and organizing existing information, making it more accessible and useful for researchers and practitioners alike.

EVIDENT
OLYMPUS

WILEY

Gradient Type-II CdSe/CdSeTe/CdTe Core/Crown/Crown Heteronanoplatelets with Asymmetric Shape and Disproportional Excitonic Properties

Farzan Shabani, Pedro Ludwig Hernandez Martinez, Nina Shermet, Hilal Korkut, Ibrahim Sarpkaya, Hamed Dehghanpour Baruj, Savas Delikanli, Furkan Isik, Emek Goksu Durmusoglu, and Hilmi Volkan Demir*

Characterized by their strong 1D confinement and long-lifetime red-shifted emission spectra, colloidal nanoplatelets (NPLs) with type-II electronic structure provide an exciting ground to design complex heterostructures with remarkable properties. This work demonstrates the synthesis and optical characterization of CdSe/CdSeTe/CdTe core/crown/crown NPLs having a step-wise gradient electronic structure and disproportional wavefunction distribution, in which the excitonic properties of the electron and hole can be finely tuned through adjusting the geometry of the intermediate crown. The first crown with staggered configuration gives rise to a series of direct and indirect transition channels that activation/deactivation of each channel is possible through wavefunction engineering. Moreover, these NPLs allow for switching between active channels with temperature, where lattice contraction directly affects the electron–hole (e–h) overlap. Dominated by the indirect transition channels over direct transitions, the lifetime of the NPLs starts to increase at 9 K, indicative of low dark-bright exciton splitting energy. The charge transfer states from the two type-II interfaces promote a large number of indirect transitions, which effectively increase the absorption of low-energy photons critical for nonlinear properties. As a result, these NPLs demonstrate exceptionally high two-photon absorption cross-sections with the highest value of 12.9×10^6 GM and superlinear behavior.

1. Introduction


Type-II heterostructures of the semiconductor nanoplatelets (NPLs) are an interesting electronic group of NPLs that provide an excellent platform for exceptional properties, such as long lifetime photoluminescence (PL), huge Stokes shift, PL wavelength tunability, and broad emission spectra, that are not possible to achieve through type-I heterostructures.^[1,2] The fundamental feature of these type-II NPLs originates from the spatial separation of the carriers to distinct domains, in which the emission happens through radiative recombination of the electrons and holes at the interface.^[3,4] To obtain this electronic structure, both the valance and conduction band of one domain must be either on a higher or lower energy level than the adjacent domain.^[5,6] In this regard, electron wavefunction mostly resides in one domain while the wavefunction of the hole is separated into the other one.

The nature of this separation, alongside with this special band alignment, causes a decrease in the recombination energy compared to the band edge energy, which shows its effect in the red-shifted emission.^[7]

For the semiconductor NPLs, the predominant Type-II heterostructure is core/crown geometry, in which the second semiconductor is laterally grown on the seed NPLs. The first type-II colloidal NPLs were synthesized via seed-mediated growth of CdTe crown on CdSe core.^[8] This chemical approach is still widely used for crown growth of either type-I or type-II core/crown NPLs, for its versatility and precision.^[9–15] Although CdSe/CdTe core/crown is the common heterostructure of interest among the type-II NPLs,^[8,16] other compositions such as CdSe/CdSeTe,^[16] CdS/ZnSe,^[17] CdTe–CdSe inverted type-II^[16] and CdSe/ZnSe dots-on-plates^[17] have also been investigated as potential heterostructures. Recently, more sophisticated heterostructures have been developed for type-II nanoplatelets with two crowns being grown on the seed core.^[18] Khan et al.^[19] proposed a two-crown heterostructure in which the intermediate

F. Shabani, N. Shermet, H. Korkut, I. Sarpkaya, H. Dehghanpour Baruj, S. Delikanli, F. Isik, H. V. Demir
UNAM – Institute of Materials Science and Nanotechnology and National Nanotechnology Research Center
Department of Electrical and Electronics Engineering
Department of Physics
Bilkent University
Ankara 06800, Turkey
E-mail: volkan@bilkent.edu.tr

P. L. H. Martinez, S. Delikanli, E. G. Durmusoglu, H. V. Demir
LUMINOUS! Center of Excellence for Semiconductor Lighting and Displays
School of Electrical and Electronic Engineering
School of Physical and Materials Sciences
School of Materials Science and Nanotechnology
Nanyang Technological University
Singapore 639798, Singapore
E-mail: hvdemir@ntu.edu.sg

 The ORCID identification number(s) for the author(s) of this article can be found under <https://doi.org/10.1002/sml.202205729>.

DOI: 10.1002/sml.202205729

crown of CdS acts as an electron barrier that inhibits the propagation of the electrons into the outermost CdTe crown. These multi-crown heterostructures are especially interesting as they offer multiple tunable recombination channels, which can be further modified toward cascade structure with bi- and tri-emission characteristics.

The characteristic feature of type-II heterostructures is the long-lived emission,^[20–25] which is induced by the charge separation that slows down the recombination at the interface of the domains. In this way, the strong Coulombic attraction between electron and hole is alleviated and the fast exciton decay is hindered, which is crucial for light-harvesting or photocatalytic applications.^[6,26] Moreover, the origin of the emission that determines the emission wavelength depends on the heterostructure's design, such as the volume, shape and composition of the domains, and the environmental condition, such as the solvent, temperature and external charge injection.^[27–29] Numerous studies have been conducted on the physics that governs the carrier dynamics in type-II heterostructures.^[30] Most of these studies investigate the carrier's dynamics through the time-correlated photon counting absorption and emission and the active radiative and non-radiative channels that determine the optical behavior.^[22]

In this study, a novel heterostructure of core/crown/crown NPLs with a step-wise band alignment was designed and synthesized through a seed-mediated one-pot technique. An analogy was drawn between the theoretical and experimental results where the geometry of the heterostructure was shown to have a critical role in the final properties of the NPLs. The intermediate crown with a staggered configuration with the core and final crown enables squeezing or loosening of the hole wavefunction and shapes the electron-hole (e–h) overlap of spatially separated charges. The recombination channel(s) can be activated by adjusting the geometry, which determines the distinguished type-II characteristics of each set of NPLs. The excitonic properties of the multi-crown type-II NPLs were shown to be sensitive to the temperature through not only the electron-phonon interaction but also the lattice contraction at low temperatures, which affects the direct recombination channels more than the indirect ones. The multi-channel gradient heterostructure exhibits a very low onset of lifetime prolongation temperature of ≈ 9 K, which indicates low excitons splitting energy promising for quantum devices. Moreover, the smooth transition between the domains facilitates lower energy photon absorption and gives rise to an extremely high two-photon absorption cross-section (δ_{2PA}) with superlinear behavior.

2. Results and Discussion

In our samples with the general heterostructure of CdSe/CdSe_{1–x}Te_x/CdTe core/crown/crown, the intermediate crown always has a band alignment with the conduction and valence band in a staggered position with respect to the core and final crown. This alignment assures that, from the energy perspective, there would be only one emission from the lowest energy path. However, as shown later, not all the samples show one peak emission, and for some samples, this dominant emission may fade away at the expense of other possible channels.

The general band alignment and all the possible transitions for core/crown/crown NPLs are shown in Figure 1a,b, respectively. The first three excitonic transitions (T_1 , T_2 , and T_3) are the intrinsic feature of each domain, which show their effect as electron–heavy hole (e–hh) and electron–light hole (e–lh) peaks in the absorption spectra of the NPLs. In that regard, the e–hh and e–lh transitions for the CdSe core are denoted as T_1 and always present themselves as two peaks located at ≈ 510 and 482 nm, respectively. For T_2 and T_3 , the e–lh transition usually fades into the absorption spectra, as shown elsewhere,^[8] and may become prominent upon overgrowth of the domain.^[31] The e–hh transition for T_2 and T_3 , on the other hand, usually shows a distinct absorption peak that depends on the lateral size and composition of the domain. The corresponding position of the peaks may be so close to each other, and for some samples, these two peaks may show their presence as only one peak; however, the emission spectra confirm the co-existence of these two domains. Alongside the direct bandgap transitions, there are three possible charge transfer (CT) channels denoted to the type-II emissions through the interfacial recombination of the excitons (Figure 1b). These three transitions are responsible for the long tail of the absorption spectra, and because of their spatially collective recombination nature, they produce a long-lived spectrally-broad emission.

The synthesis route of these multi-crown NPLs is demonstrated in Figure 1c. Starting with four monolayers (MLs) CdSe core, the first crown was grown via the introduction of an anion mixture with the desired ratio of Se and Te alongside the Cd precursor. After a brief resting time, the second precursor of only-Te was injected into the solution to form the CdTe final crown (see the Methods for the details). This approach allows us to tune the composition and size of the crowns in a relatively simple manner and engineer the final multi-crown heterostructure. The X-ray photoelectron spectroscopy (XPS) spectra of CdSe/CdSeTe/CdTe core/crown/crown NPLs for three participant elements of Cd, Se, and Te are shown in Figure S4, Supporting Information. The excellent fit for the elements and the binding energies suggest no formation of unwanted species, or even if, they were cleared out from the ensemble after the cleaning procedure. This is especially important for the chalcogenides with a higher tendency to form unwanted subspecies.^[32,33] The X-ray diffraction (XRD) pattern of the NPLs with two different ratios of the intermediate crown is shown in Figure S5, Supporting Information. As the share of the final crown increases, the peaks tend to shift to lower diffraction angles due to the larger lattice constant of CdTe compared to CdSe. The optical properties of the NPLs arise from the interactive combination of all the transitions discussed. Due to the constant thickness of the core, core/crown and core/crown/crown NPLs, the volume of the domains is proportional to their surface area and lateral size, which in turn depends on the injected amount of Se-Te and Te precursors. In our study, we investigate the effect of three parameters, namely, the ratio of the crowns, the intermediate crown composition and the overall size of two crowns on the electron and hole wavefunctions and the recombination dynamics in the NPLs. In the first step, we synthesized multi-crown type-II NPLs with similar compositions of the intermediate crown but having various lateral sizes. The overall size of the intermediate

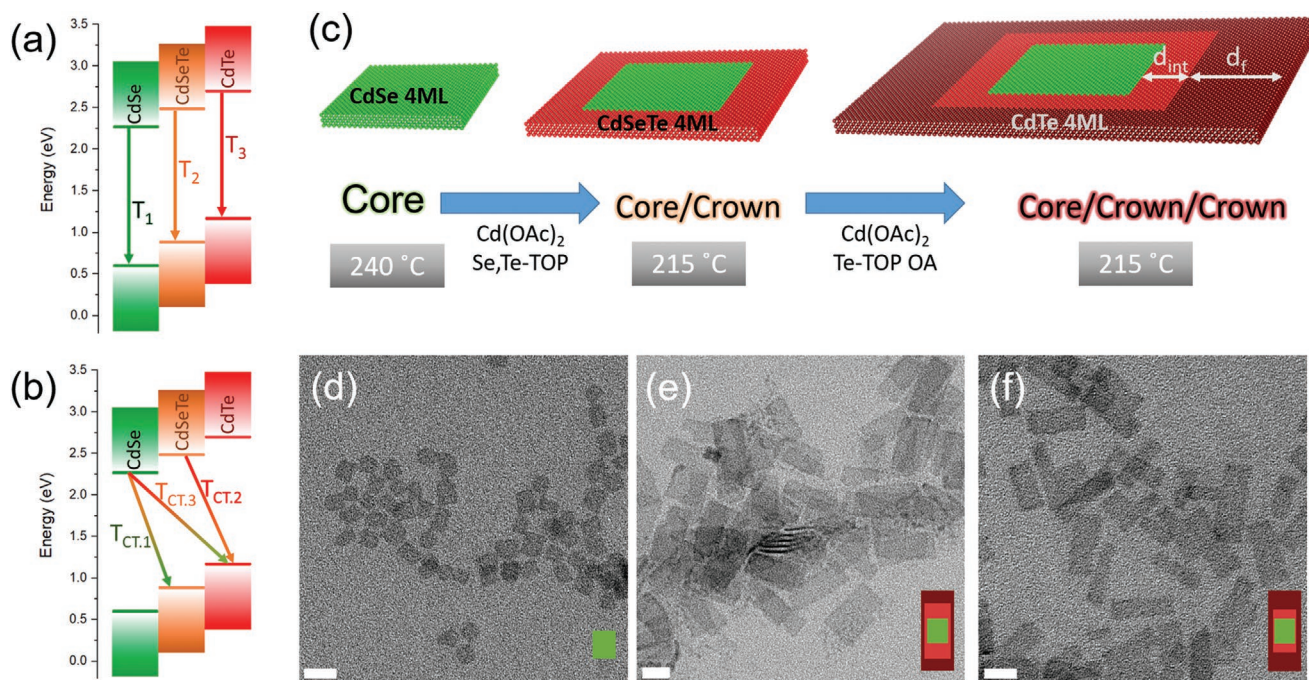


Figure 1. a) Band alignment of the NPLs with the general heterostructure of CdSe/CdSeTe/CdTe core/crown/crown and all the possible direct band-edge transitions happen in one domain. b) Same as (a) for the possible indirect type-II transitions between two different domains. c) A schematic of the synthetic route of CdSe/CdSeTe/CdTe core/crown/crown NPLs. Starting with four monolayers (MLs) CdSe core, two consecutive crowns were grown through a single-pot procedure where a mixture of Se-Te was injected for the first crown and then only Te was introduced to the NPLs. d) TEM image of 4 MLs CdSe core and e, f) multi-crown NPLs with r equal to 3 and 0.33, respectively. All scale bars are 20 nm.

and final crown was kept constant, while their longitudinal ratio ($r = d_{\text{int}}/d_{\text{f}}$, where d_{int} and d_{f} are the longitudinal length of the intermediate crown and final crown, respectively, shown in Figure 1c) varied to be 1/3, 1/1, and 3/1 through adjusting the injected amount of precursors. Figure 1d shows the transmission electron microscopy (TEM) image of the original core before the crown growth, where NPLs have a square shape with a lateral size of $12.1 \pm 1.5 \times 10.6 \pm 1.5 \text{ nm}^2$. After the growth of the CdSeTe/CdTe crown, the symmetry of NPLs is disturbed, with one of the facets growing faster than the other one. These rectangular core/crown/crown NPLs have a lateral size of $16.1 \pm 0.8 \times 39.3 \pm 3.6 \text{ nm}^2$ for the case of $r = 3/1$ (Figure 1e), and their size does not significantly change when r is changed to 1/3 (lateral size was measured as $17.9 \pm 0.9 \times 42.6 \pm 3.8 \text{ nm}^2$ for the corresponding NPLs in Figure 1f). The slight change in the lateral size for these two sets of NPLs suggests very similar growth kinetic of the crowns regardless of the anion. Moreover, the huge break in the symmetry of the NPLs points to the intrinsic anisotropic growth mechanism from the length to the width of the NPLs. The growth dynamics of the NPLs and the composition of the domains are discussed in Figures S6 to S9, Supporting Information. The absorption and emission spectra of these NPLs are shown in Figure 2a,b, respectively. For $r = 1/3$ and 1/1, the absorption spectra show two peaks at 583 and 560 nm originating from the $\text{CdSe}_{0.5}\text{Te}_{0.5}$ and CdTe domains, respectively. The e-hh absorption peak for 4 MLs CdTe domain in the case of only CdTe core and CdSe/CdTe core/crown NPLs has been reported to be at the same wavelength.^[34,35] Incorporation of selenium in the intermediate crown has the alloying effect and it should blue-shift the e-hh

of the CdSeTe domain.^[36] However, while CdSe has a higher bandgap than CdTe, the shift caused by Se is due to a phenomenon known as “optical bowing.”^[37]

While for most semiconductor alloys, the physical properties, such as lattice constant, varies linearly with composition, the same behavior is not applicable for bandgap energy.^[37,38] The bowing behavior of the bandgap energy can be best described by $E_{\text{BG}}(x) = xE_{\text{BG}}^{\text{A}} + (1-x)E_{\text{BG}}^{\text{B}} - bx(1-x)$, where $E_{\text{BG}}(x)$, E_{BG}^{A} and E_{BG}^{B} are bandgap energies of the semiconductor alloy and pure semiconductor A and B, respectively, and b is the optical bowing parameter.^[38] The quadratic term causes deviation from linear behavior and in the case of CdSeTe alloy semiconductor, decreases its bandgap energy.^[39] The origin of optical bowing is the long-range disorder in the lattice structure, which brings in locally active parameters affecting the bandgap but not the lattice constant. The change in the bandgap energy is mainly due to the varying tetrahedral bonding angle of Se/Te and Cd and different charge distributions on the anions originating in different electronegativity.^[40] This effect is responsible for the nonlinear change in the e-hh peak position and has been reported to have a strong influence on CdSeTe alloys.^[41] The absorption peak of CdSeTe intermediate crown in our heterostructure closely correlates with the previous reports of CdSe/CdSeTe core/crown NPLs in the literature.^[31,42] With increasing the size of the intermediate crown, the original e-hh peak of CdTe has been dissolved into the spectrum (for $r = 3/1$), which we believe is due to the optical bowing and lattice strain exacerbation that can be a source for optical nonlinearity.

A dual emission PL is recorded for all three sets of NPLs with varying r ; however, the peak profile, including position,

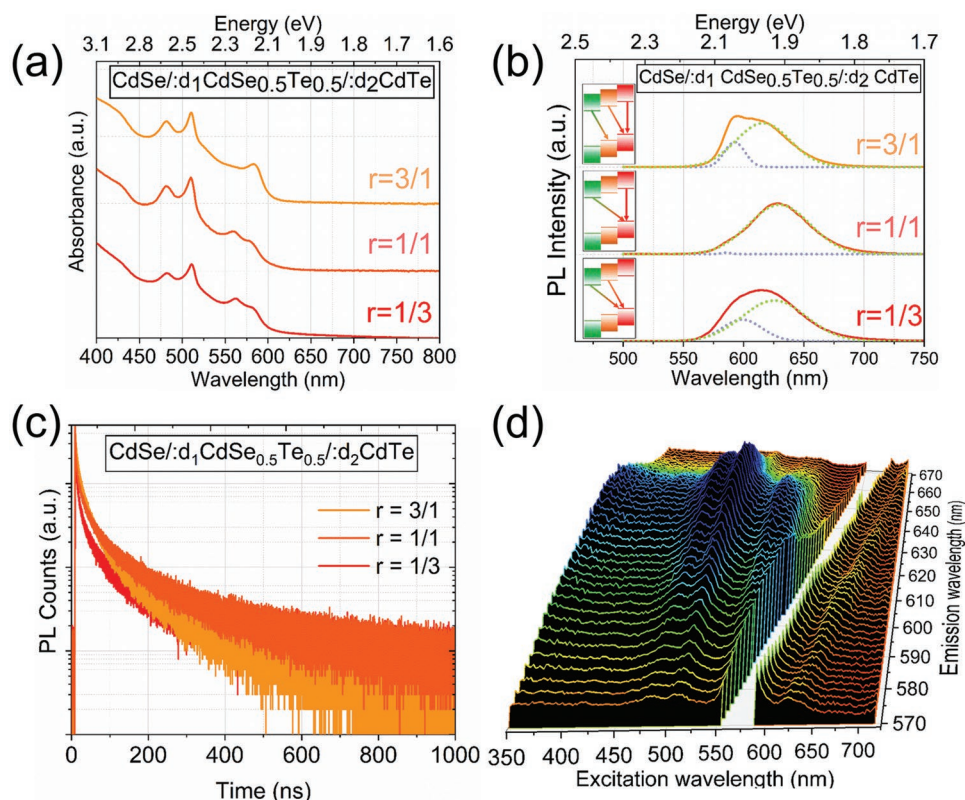


Figure 2. a) Absorption profile of CdSe/CdSeTe/CdTe core/crown/crown NPLs with constant composition of the intermediate crown (Se/Te = 1) and changing ratio of intermediate to final crown, r . b) PL profile of the same samples. The dotted curves are the deconvoluted peaks for each graph. c) TRF decay curves at the emission peak wavelength of the NPLs. d) PLE profile of the NPLs with $r = 1$ sweeping from the beginning (570 nm) to the end (670 nm) of the emission spectra.

linewidth, and peaks ratio, differs drastically for different architectures. Deconvolution of PL spectra can help to explain the origin of the emission for these multi-peak emission NPLs. The deconvoluted emission peaks for $r = 1/3$, $1/1$, and $3/1$ are shown in Figure S10, Supporting Information. For NPLs with $r = 3/1$, one of the fitted peaks is much narrower with full-width-at-half-maximum (FWHM) of 20 nm than the other one (with FWHM of 53 nm). This narrow and higher-energy emission peak is originated from the direct recombination within one domain and has a smaller Stokes shift than the broader peak. The bicolor emissive type-II heterostructure has been reported previously for CdSe/CdSe_xTe_{1-x} core/crown NPLs;^[31] however, the same heterostructure in other studies shows only one emission profile when the lateral size of the crown is sufficiently large enough.^[42] The reason behind these seemingly contradictory results is originated in the sensitive nature of type-II NPLs to the environment and complicated interfacial recombination dynamics. As a result, the interfacial recombination is not only dependent on the energy level of each transition but is also extremely sensitive to the size of each domain and the absolute recombination area within the nanocrystal. The configuration of locally excited exciton plays a critical role in coupling/decoupling of the neighboring exciton by Coulomb interaction and whether to block or allow specific transitions.^[29] These interactions are more sophisticated for a two-crown structure, which can also spatially decide on the distance of the electron

and hole and make up a dual emission. The change in the PL spectra of the samples with different architectures emphasizes the switch from one transition channel to another. The decay curves, shown in Figure 2c, help to reveal the dynamics behind the recombination and the active emission channel(s). The sample with $r = 3/1$ shows the fastest recombination rate, and with decreasing the intermediate crown size (d_{int}), the recombination slows down (decay components and lifetimes are summarized in Table S2, Supporting Information). This was not predictable as the recombination distance of electron and hole in the final crown and core is increased, and it should take a longer time for them to recombine. Moreover, when the intermediate crown size further decreases, the recombination rate does not increase for $r = 1/3$ compared to $r = 1/1$.

Deconvolution of the peaks for NPLs with $r = 3/1$ showed the emergence of a distinct narrow peak, which is attributed to the direct recombination in the final CdTe crown, T_3 . The time-resolved fluorescence (TRF) measurement now further confirms this assumption that an element of fast-decaying recombination is due to the band-edge transition in one domain. In other words, when the separation distance of electron and hole is extensively increased, the probability of band-edge recombination of electron and hole in one domain also increases. For NPLs with $r = 1/1$, some portion of this T_3 transition exists, which indicates that the distance is still large enough, while for $r = 1/3$ NPLs, the short spatial distance of

electron-hole completely turns the equilibrium in favor of type-II recombination. The minuscule change in the intensity-averaged luminescence lifetime (τ_{avg}) for $r = 1/1$ and $1/3$ NPLs also points out to the shorter $T_{\text{CT},3}$ recombination distance of $r = 1/3$ NPLs versus fast band-edge recombination of $r = 1/1$ NPLs. The decay curves collected at two emission wavelengths of 577 and 627 nm for NPLs with $r = 1/3$ (shown in Figure S11, Supporting Information) indicates that the recombination rate at lower wavelength is approximately two times faster than the longer wavelength, which suggests the activation of other type-II transition such as $T_{\text{CT},2}$.

The photoluminescence excitation (PLE) for the sample with $r = 1/1$ is recorded for emissions between 570 and 670 nm and is presented in Figure 2d. For all of the emission wavelengths, the e-hh and e-lh peaks of the core are in position and two peaks of the crowns can be detected, which shows that both crowns are actively responsible for the final type-II emission and the apparent emission at all wavelengths is not due the two different ensembles of NPLs. Based on the TEM images, the NPLs were shown to have a lateral size distribution, which can affect the active recombination channel. For core NPLs, the distribution accounts for 14.1% in the longitudinal direction and by growing two crowns, this distribution is decreased to 9.1% (for multi-crown NPLs with $r = 3/1$), showing a more homogenous growth of the crowns. This also shows that a big portion of the size inhomogeneity is coming from the core, while the crowns are more homogeneous in size. In an extreme case, the size distribution of the NPLs can account for part of the multi-channel emission of the NPLs by providing a mixture of two ensembles with different active recombination channels. However, throughout our experiments, the change in r from $1/3$ to $1/1$ and $3/1$ corresponds to 25% change in the size of the crowns, which is well above the overall size distribution of the NPLs. Hence, the switches between active channels are principally due to the change in the absolute domain size. The lateral size distribution can increase the FWHM of the emission lines and contribute to peak broadening.

The extreme variation in the recombination behavior points out the great sensitivity to the size of the intermediate crown. In a broader image, the conditioning of electron and hole landscape, where both are energetically separated into different domains and then spatially recombined, decides on the preferred transition channel. The TEM images showed that after the growth of the crowns, the shape of the NPLs changes from square to rectangular. To better understand the recombination dynamics in these type-II rectangular NPLs, we further calculate the electron and hole wavefunction distribution and its dependency on the geometry of the NPLs, considering the problem of a particle in a box in 2D. While for both square and rectangular geometries, the electron charge density remains in the core, the asymmetric shape of the multi-crown NPLs brings a disproportional hole charge density with a dominant fraction on the longitudinal edges of the final crown instead of the corners in the case of square geometry (Figure S12, Supporting Information). The electron and hole wavefunctions remain their center of position in the core and final crown, respectively, and only for higher state energies, they may diffuse into the intermediate crown or narrower edges (Figure S13, Supporting Information). The dependency of the electron and hole wavefunctions on

the geometry of the multi-crown NPLs is shown in Figure 3a. The electron wavefunction does not show any change with r due to the consistency of the core size with the lowest energy (see Figure 1a). However, as the size of the intermediate crown increases, which can be translated as a smaller final crown, the hole wavefunction gradually squeezes in a smaller area. The indirect type-II recombination is the result of the overlap between the two wavefunctions. The e-h overlap versus r for three different compositions of $\text{CdSe}_{1-x}\text{Te}_x$ intermediate crown is demonstrated in Figure 3b, where regardless of the composition, the overlap decreases with increasing r . As we squeeze the hole wavefunction through changing r , we decrease the probability of the excitons interacting with each other at different domains; hence, the chance of direct recombination will increase, as was seen in the PL profile of the samples (Figure 2b and Figure S10, Supporting Information).

In calculating the electron and hole wavefunction distributions, the band alignment of the heterostructure was assumed to be unstrained. However, the difference between the lattice constant of the domains causes a strain, which can bend the conduction and valance band and make a local potential barrier or well in the band structure of semiconductor heterojunctions.^[43,44] The direct recombination channel in the CdTe domain points to the retention of the electron in the domain and, later, its direct recombination. Bicolor emission was previously observed for $\text{CdSe}/\text{CdSe}_{1-x}\text{Te}_x$ core/crown NPLs, in which at crown compositions near to $x = 0.5$, an emission line related to the CdSeTe domain emerges.^[31] The strain-induced local barrier in the conduction band can prevent the electron from transferring to its lowest energy state in the CdSe domain. This strain should increase by decreasing the CdSeTe buffer layer size and amplifying the CdTe emission. However, with decreasing the size of the intermediate crown, the share of the CdTe emission decreases and then completely diminishes for $r = 1/3$. The observation shows that the local barrier preventing the electron transfer is not the only cause of the switching between the channels and probably not the main reason behind the retention of the electron.

Initially, the hot electron and hole do not feel the band structure; however, the electron with a lower effective mass relaxes faster than the hole. The direct recombination of retained electron and hole in the CdTe domain has a much higher rate (in the order of ns with components as fast as hundreds of picoseconds)^[11] than the indirect recombination, which requires the spatial transfer of the charges. As the size of the intermediate crown increases ($r = 3/1$), the e-h overlap decreases and the transfer of both electron and hole to the intermediate crown becomes harder. Previously, it was shown that the carrier transfer for $\text{CdSe}/\text{CdTe}/\text{CdSe}$ core/crown NPLs with two type-II interfaces is unusually long, in the order of hundreds of ps, showing a hindrance in the formation of the charge-separated state.^[18] Also, in CdSe/CdTe core/crown NPLs, the carrier transfer from CdTe and CdSe domains can take up to 100 ps.^[45] The comparable direct recombination and carrier transfer lifetimes in a type-II system enable direct recombination before charge separation. After investigating the effect of the geometry of the crowns, we focus on the effect of the intermediate crown composition on the recombination dynamics. Herein, we changed the composition of the intermediate

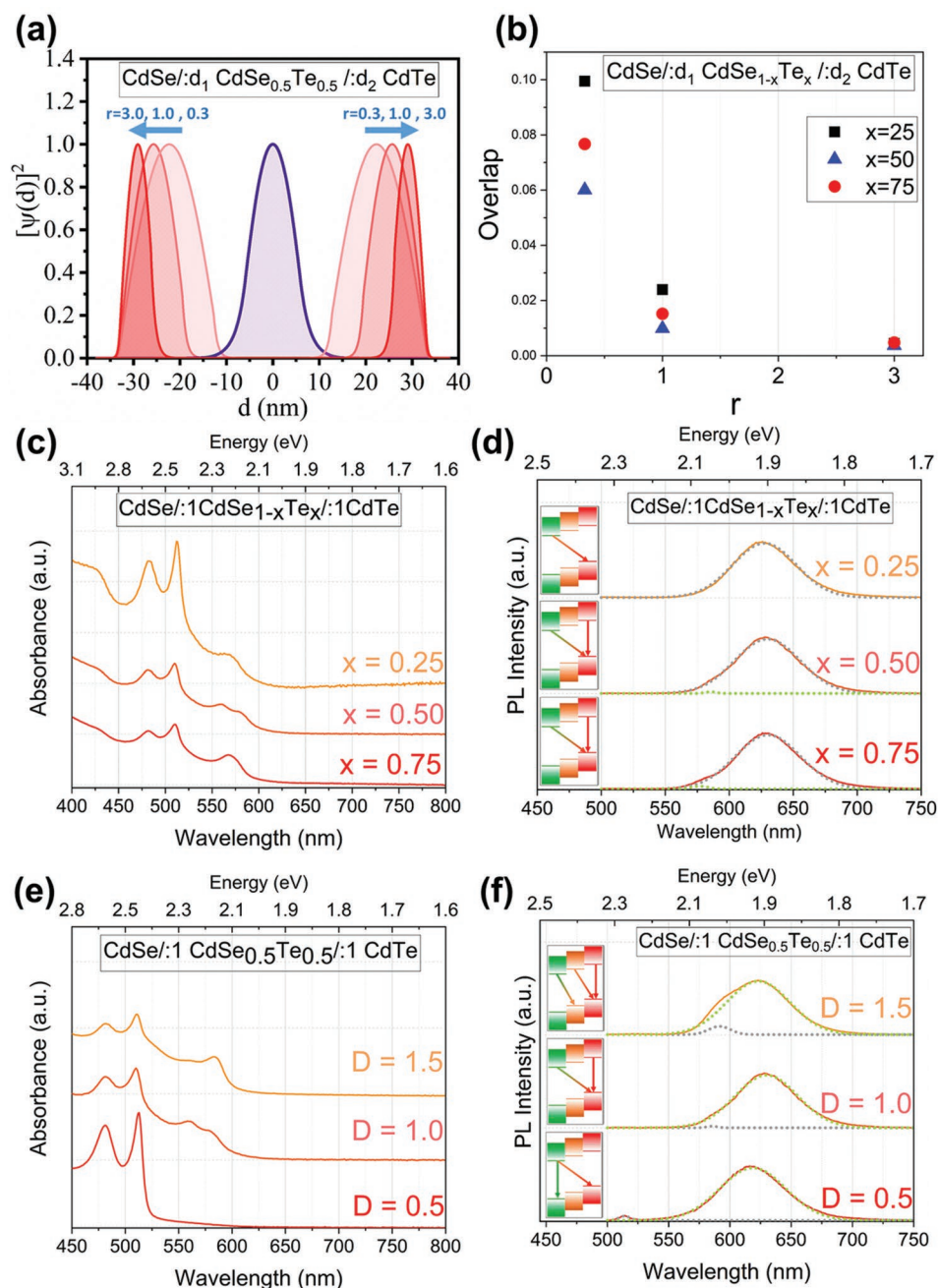


Figure 3. a) The electron (purple) and hole (red) wavefunctions of the NPLs with $x = 0.5$ and changing r . b) The e-h overlap extracted from the corresponding heterostructures with different r and x . c) Absorption and d) PL spectra of the CdSe/CdSe_{1-x}Te_x/CdTe core/crown/crown NPLs with different intermediate compositions. e) Absorption and f) PL spectra of the CdSe/1 CdSe_{0.5}Te_{0.5}/1 CdTe core/crown/crown NPLs with different collective sizes of the crowns, $D = d_{int} + d_f$.

crown from selenium-rich to tellurium-rich at constant $r = 1/1$. Figure 3c,d show the absorption and emission spectra of three samples with nominal compositions of $x = 0.25$, 0.50 , and 0.75 , respectively, in which x is the fraction of Te. As the Se concentration increases, the share of the absorbance proportion corresponding to the CdSe e-hh peak increases relative to CdTe e-hh absorption peak. This increase is due to the smooth and gradually decreasing CdSeTe alloyed crown peak at high selenium concentrations, shown for CdSe/CdSeTe

core/crown heterostructure before^[31] and makes the share of CdSe core peak stronger than the crown. Increasing the amount of Se widens the bandgap of CdSeTe alloyed semiconductor with some levels of bowing effect for the composition of Te higher than 30%.^[28,46] The emission spectra of the samples seem to be almost the same for all three compositions, which strongly suggests no switch in the active transition channel. The results show that it is the size of the intermediate crown that decides on the active transition and final recombination

dynamics of the NPLs, regardless of their composition. The theoretical calculations results, depicted in Figure 3b, suggests that at higher r , the composition of the intermediate crown has little to no effect on the e–h overlap, and only at low r it becomes decisive. Considering the long e–h separation distance, the result makes perfect sense, as the overlap is already decreased and just at short distances changing the band alignment becomes a prominent parameter. One significant complication arising from the theoretical calculation is that the NPLs with $x = 0.5$ possess the lowest overlap. The intermediate crown tends to act more like a CdSe core or CdTe crown at boundary compositions. Hence, as the elemental fraction of Te in the intermediate crown gets closer to zero or 1, the prospect of indirect $T_{CT,3}$ recombination becomes stronger, and for the molar fraction of Te (x) equal to 0.5, the intermediate crown has the least nature of the core or final crown. The decay curves of the samples with different intermediate compositions are shown in Figure S14, Supporting Information. In line with the previous observations, NPLs with $x = 0.5$ have the fastest decay rate compared to $x = 0.25$ or 0.75 indicating the least type-II characteristic of the sample.

Until now, the collective size of the crowns was kept constant and it was only the ratio of d_{int}/d_f that was changed. To investigate the absolute effect of crown size, we changed the collective size of the crowns, $D = d_{int} + d_f$. As the hole wavefunction only resides on the smaller edges of the NPLs, it is only the longitudinal length of the multi-crown NPLs that was taken into account. Based on the TEM images of the samples shown in Figure 1d–f, the absolute collective size of the crowns in the longitudinal direction is 28.8 nm, which is designated as $D = 1.0$. With changing the amount of anion precursor injected, two sets of multi-crown NPLs with $D = 0.5$ (14.4 nm) and $D = 1.5$ (43.2 nm) were also synthesized. The relative size of the collective crowns to the core for these NPLs are 1.2, 2.4, and 3.8 for $D = 0.5$, 1.0, and 1.5, respectively. The absorption and emission spectra of three samples with the same r of 1 and the same intermediate crown composition of $x = 0.50$ but different D is shown in Figure 3e,f. When D is too small, complete interfacial separation of electron and hole does not happen, and instead, a small emission peak of CdSe emerges at 512 nm. The absorption spectrum does not show any distinct crown peak, and instead, a long tail of charge transfer extends from the e–hh peak of CdSe to the lower energy side of the spectrum. As D increases, the absorption peaks of the two crowns become apparent, and a second peak starts to emerge for $D = 1.0$. The decay curves of the NPLs in Figure S15, Supporting Information, show that for the smallest collective crown size, recombination is slower than for bigger collective crowns with $D = 1.0$ and 1.5. This phenomenon is due to the change in the preferred recombination pathway of electron and hole. For the NPLs with larger crowns, once dormant transition channels ($T_{CT,1}$ and $T_{CT,2}$) become more and more favorable over the least energy channel of $T_{CT,3}$. For these channels with no interspace, electron and hole travel over a shorter distance, which causes a faster recombination dynamic and hence a shorter lifetime. Deconvolution of the PL peaks in Figure S16, Supporting Information shows that the direct recombination transition channel (with FWHM of 21.6 nm) for $D = 1.5$ is stronger than the case of $D = 1$ (Figure S10, Supporting Information), while NPLs with

$D = 0.5$ are the only ensemble with direct recombination at CdSe core with an emission peak wavelength of 513.8 nm.

The same argument about the electron retention in the CdTe crown can be used to explain the retention of the hole in the CdSe core, which makes up for the CdSe emission. For small NPLs with $D = 0.5$, the bicolor PL profile consists of one CdSe band-edge emission and one type-II emission. With increasing D , the band-edge emission diminishes (Figure 3f), similar to the previous report of CdSe/CdTe core/crown NPLs.^[47] Increasing the size of the crown would increase the lattice strain and hence put the hypothetical potential barrier in the conduction band at a higher level. However, for both of the observations enlarging the crown lead to diminish of the CdSe emission, which means the potential barrier is not the leading cause of CdSe emission. We believe that, although lattice strain can change the electron and hole potential landscapes, but the leading effect in the final e–h overlap is the geometry of the NPLs. For small-crown NPLs a higher fraction of holes is statistically generated in the core region than in the crowns. Also, the direct recombination lifetime in the CdSe domain is fast, which gives a chance to small portion of the holes in CdSe to recombine directly before the carrier transfer to the interface and separation takes place.

Incorporation of an intermediate crown changes the band alignment of the NPLs, in which the predominant transition is dependent on the relative size of the crowns, the overall size of the crowns, and to some extent, on the energy level of the intermediate crown. In order to gain further insight into the recombination dynamics, we followed the temperature-dependent PL of CdSe/3 CdSe_{0.5}Te_{0.5}/1 CdTe NPLs, which are shown to have two emission peaks: one direct band-edge and one indirect type-II. The relative emission intensity of the two peaks is different from what was recorded in Figure 2b due to the change in the dielectric medium after the transfer of the NPLs from solution to drop-casted film.^[29] Figure 4a follows the PL spectra at different temperatures. The PL peak wavelength (Figure 4b) blue-shifts upon decreasing the temperature due to the lattice contraction of the nanocrystal; however, the NPLs demonstrate a strange switch from dual emission to single emission. While for temperatures above 250 K, two emission peaks are resolvable, one of the peaks fades away with a further decrease in the temperature. The peak deconvolution for the first three temperatures of 295, 250, and 200 K is demonstrated in Figure S18, Supporting Information. The change can also be tracked from the sudden drop in the PL FWHM from 250 to 200 K presented in Figure S19, Supporting Information. This behavior shows that the indirect type-II recombination channel dominates over the other competitive direct recombination channel at the CdTe crown, T_3 . Conclusively, the direct recombination of the multi-crown type-II NPLs is the result of a sufficiently big intermediate crown and thermal activation.

The sudden deactivation of the direct transition channel has almost no effect on the evolution of the type-II emission peak versus temperature (Figure 4b), where the peak linearly blue-shifts as temperature decreases. Upon fitting the PL wavelength with Varshney semiempirical equation^[48] and Bose–Einstein-type equation,^[49] both known to best explain the bandgap energy with temperature, the values obtained for Debye temperature demonstrate high uncertainty and are far

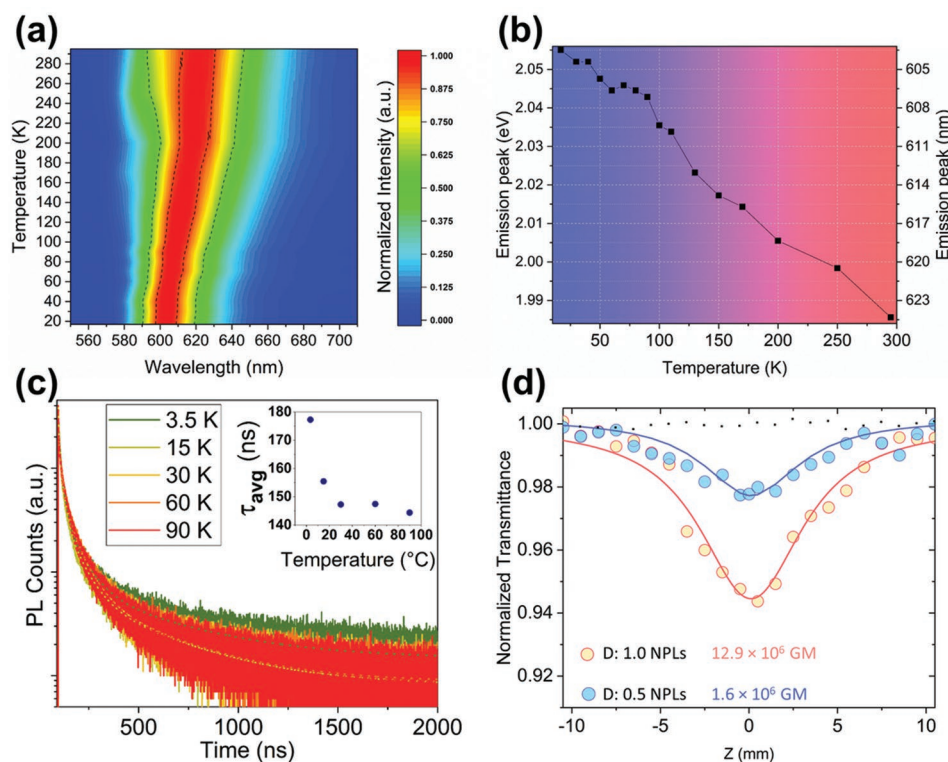


Figure 4. a) Temperature-dependent PL spectra at different temperatures and b) emission peak position versus temperature extracted from the PL spectra for CdSe/3 CdSe_{0.5}Te_{0.5}/1 CdTe core/crown/crown NPLs. c) PL decay curves for the same samples. The inset shows the evolution of the lifetime with temperature. d) Open-aperture z-scan graphs comparing two samples of multi-crown NPLs with the same composition ($x = 0.5$) and $r = 1$ and different collective crown sizes, D . The black scatter dots correspond to the measurement for only hexane, and the solid lines are the fittings for the samples. An increase in the size of the NPLs gives a huge rise in the two-photon absorption cross-section from 1.6×10^6 to 12.9×10^6 GM.

below the prediction (see the supporting information). Negative deviation in Debye temperature has been shown for QDs compared to the bulk semiconductor and was attributed to the size dependency of the vibration of confined phonons, which decreases in frequency upon reducing the size.^[49] However, for the present work, the reason behind the low estimation of the Debye temperature is the positioning of different lattices with different oscillator energies, which leads to low Debye temperatures for each component with high deviation.^[12,50] The linear dependency predicts that the exciton-phonon interaction is negligible in a broad range of temperatures, and the lattice contraction plays a bigger role in the indirect bandgap recombination of electron and hole. This was foreseeable as we show that the separated electron and hole are too sensitive to the interspacing between the core and final CdTe crown.

As one of the powerful tools to understand the recombination dynamics and properties of the excitons, we also measured the temperature-dependent TRF.^[51] Figure 4c shows the decay curves for CdSe/3 CdSe_{0.5}Te_{0.5}/1 CdTe multi-crown NPLs at low temperatures, which were fitted with a four-exponential function as the emission is originated from different type-II channels. The average lifetime (τ_{avg}) of the sample slightly increases with decreasing temperature for $T > 15$ K; however, a sharp increase in τ_{avg} from 155 to 177 ns occurs when T is further decreased from 15 to 3.5 K. The energy splitting (Δ) induced by the e-h exchange is responsible for the increase in the lifetime at low T , where the dark state (quasi-forbidden

spin) with the lowest exciton energy level comes into effect.^[52,53] The dark state, in oppose to the bright state (spin allowed), has a much longer lifetime, which upon prevention of thermal activation at temperatures corresponding to $k_B T < \Delta$ (k_B is the Boltzmann constant) becomes effective.^[54,55] Previously, it was shown that for the CdTe/CdS core/shell QDs, the lifetime stays almost constant between 20 to 120 K.^[48] The same behavior was also reported for 4 MLs CdSe/CdTe core/crown NPLs except that at $\approx T > 40$ K, lifetime starts to decrease, with two distinctly opposing bright and dark decay components.^[56] In our case, the sudden increase in the lifetime comes at a much lower T ; moreover, only the longest lifetime component shows a meaningful increase while the rest stay almost constant (Figure S21, Supporting Information). As one of the requirements of quantum devices where it is crucial to minimize the fine structure splitting and depletion of dark excitons,^[57,58] these multi-crown type-II heterostructures offer an adjustable alternative quantum system where e-h overlap dominates the e-h exchange reaction and hence the splitting.^[59,60] As we showed, with the implementation of the intermediate crown, the splitting can be finely tuned through the size and composition of the intermediate crown. Type-II electronic heterostructure with direct and indirect transitions is known to have strong nonlinear properties necessary for photon upconversion.^[19,61,62] Also, 2D NPLs are known for their intrinsically large linear absorption cross-section and giant oscillator strength compared to their QD counterparts.^[63] As one of the essential prerequisites of

nonlinear properties, the nanocrystal must have a high two-photon absorption cross-section (δ_{2PA}) where it can readily absorb photons with energies lower than the bandgap. One frequently used strategy in type-II heterostructures is benefiting from the lower energy charge transfer state. Herein, instead of directly exciting an electron in one of the domains, the e-h pair is formed as a mixed process of relative delocalization of electron via charge transfer with the first incident photon and then complete delocalization with the second incident photon. To assess the δ_{2PA} of our NPLs, we performed an open-aperture z-scan with an excitation wavelength (λ_{ex}) of 800 nm (the details are provided in the Supporting Information) on two sets of NPLs with identical composition ($x = 0.5$) and $r = 1$, and different D . For our multi-crown type-II NPLs with $r = 1$ and lateral size of 634 nm², δ_{2PA} was measured to be 12.9×10^6 GM, the highest reported number for Cd-based nanocrystals to the best of our knowledge.^[64,65] Smaller NPLs with $D = 0.5$ demonstrate drastically lower δ_{2PA} of 1.60×10^6 GM. It was previously shown that the lateral size, and consequently the volume of the NPLs, is a critical factor;^[65,66] however, the change in the size of our NPLs was small. For example, for type-I NPLs, the highest reported δ_{2PA} was 2.247×10^6 GM, corresponding to 4 MLs CdSe core NPLs with a lateral size in the order of 25 000 nm², whereas the same NPLs with 2.5 times smaller lateral size had almost 4.5 times lower cross-section, both values in the same order. We showed that smaller NPLs ($D = 0.5$) possess less of a type-II electronic structure characteristic, apparent from their absorption profile, while NPLs with $D = 1$ had two prominent crown peaks. The observation reveals the critical effect of type-II electronic structure on the nonlinear properties above the conventionally known parameter of size^[65,66] and apparent superlinear behavior of these heterostructures.

3. Conclusion

In summary, we demonstrate the design and synthesis of gradient type-II CdSe/CdSeTe/CdTe core/crown/crown NPLs and investigate their excitonic properties. The unique electronic heterostructure of these NPLs gives rise to multiple of direct band-edge and indirect type-II channels where upon adjusting the intermediate crown, the e-h wavefunctions and the overlap between them can be adjusted, and the optical properties can be tuned. The geometry of the NPLs exhibits a far more critical factor in the final optical properties and activation/deactivation of the channels compared to the composition of the intermediate crown. We showed the sensitive nature of the active channels to the temperature that besides the conventional electron-phonon interaction, the lattice contraction can also change the overlap and hence the final emission properties. The low-temperature decay behavior of the NPLs revealed a very low dark-bright exciton splitting energy, which is originated in the localization of the electron and hole at the interface of the domains where electrons and holes can readily recombine from the many existing indirect channels. Moreover, the NPLs demonstrate an exceptionally high two-photon absorption cross-section of 12.9×10^6 GM, which scales superlinearly with the volume of the NPLs. The result further encourages the design and usage of the gradient type-II heterostructures, especially

for nonlinear applications of photodetectors, bioimaging and quantum devices.

Supporting Information

Supporting Information is available from the Wiley Online Library or from the author.

Acknowledgements

The authors gratefully acknowledge the financial support from Agency for Science, Technology and Research (A*STAR) MTC program, Grant No. M21J9b0085 (Singapore), Ministry of Education Tier 1 grant MOE-RG62/20 (Singapore) and TUBITAK 115F297, 117E713, 119N343, 121N395, and 20AG001. H.V.D. also acknowledges the support from TUBA.

Conflict of Interest

The authors declare no conflict of interest.

Data Availability Statement

The data that support the findings of this study are available from the corresponding author upon reasonable request.

Keywords

colloidal quantum wells, semiconductor nanoplatelets, two-photon absorption, wavefunction engineering

Received: September 16, 2022

Revised: December 22, 2022

Published online: January 17, 2023

- [1] A. P. Alivisatos, *J. Phys. Chem.* **1996**, *100*, 13226.
- [2] A. M. Smith, S. Nie, *Acc. Chem. Res.* **2010**, *43*, 190.
- [3] S. Kim, B. Fisher, H. J. Eisler, M. Bawendi, *J. Am. Chem. Soc.* **2003**, *125*, 11466.
- [4] C. H. Chuang, S. S. Lo, G. D. Scholes, C. Burda, *J. Phys. Chem. Lett.* **2010**, *1*, 2530.
- [5] D. Mourad, J. P. Richters, L. Gérard, R. André, J. Bleuse, H. Mariette, *Phys. Rev. B: Condens. Matter Mater. Phys.* **2012**, *86*, 1.
- [6] S. S. Lo, T. Mirkovic, C. H. Chuang, C. Burda, G. D. Scholes, *Adv. Mater.* **2011**, *23*, 180.
- [7] R. G. Chaudhuri, S. Paria, *Chem. Rev.* **2012**, *112*, 2373.
- [8] S. Pedetti, S. Ithurria, H. Heuclin, G. Patriarche, B. Dubertret, *J. Am. Chem. Soc.* **2014**, *136*, 16430.
- [9] S. Delikanli, O. Erdem, F. Isik, H. D. Baruj, F. Shabani, H. B. Yagci, E. G. Durmusoglu, H. V. Demir, *J. Phys. Chem. Lett.* **2021**, *12*, 2177.
- [10] M. D. Tessier, P. Spinicelli, D. Dupont, G. Patriarche, S. Ithurria, B. Dubertret, *Nano Lett.* **2014**, *14*, 207.
- [11] L. T. Kunneman, J. M. Schins, S. Pedetti, H. Heuclin, F. C. Grozema, A. J. Houtepen, B. Dubertret, L. D. A. Siebbeles, *Nano Lett.* **2014**, *14*, 7039.
- [12] V. Steinmetz, J. I. Climente, R. Pandya, J. Planelles, F. Margailan, Y. Puttisong, M. Dufour, S. Ithurria, A. Sharma, G. Lakhwani,

- L. Legrand, F. Bernardot, C. Testelin, M. Chamarro, A. W. Chin, A. Rao, T. Barisien, *J. Phys. Chem. C* **2020**, 124, 17352.
- [13] Q. Li, K. Wu, J. Chen, Z. Chen, J. R. McBride, T. Lian, *ACS Nano* **2016**, 10, 3843.
- [14] E. Ebrahimi, M. Irfan, F. Shabani, Y. Kocak, B. Karakurt, E. Erdem, H. V. Demir, E. Ozensoy, *ChemCatChem* **2020**, 12, 6329.
- [15] S. Delikanli, F. Isik, F. Shabani, H. D. Baruj, N. Taghipour, H. V. Demir, *Adv. Opt. Mater.* **2021**, 9, 2002220.
- [16] A. V. Antanovich, A. V. Prudnikau, D. Melnikau, Y. P. Rakovich, A. Chuvilin, U. Woggon, A. W. Achtstein, M. V. Artemyev, *Nanoscale* **2015**, 7, 8084.
- [17] S. Yadav, A. Singh, S. Sapra, *J. Phys. Chem. C* **2017**, 121, 27241.
- [18] C. Dabard, V. Guilloux, C. Gréboval, H. Po, L. Makke, N. Fu, X. Z. Xu, M. G. Silly, G. Patriarche, E. Lhuillier, T. Barisien, J. I. Climente, B. T. Diroll, S. Ithurria, *Nat. Commun.* **2022**, 13, 5094.
- [19] A. H. Khan, G. H. V. Bertrand, A. Teitelboim, C. M. Sekhar, A. Polovitsyn, R. Brescia, J. Planelles, J. I. Climente, D. Oron, I. Moreels, *ACS Nano* **2020**, 14, 4206.
- [20] W. Y. Wu, M. Li, J. Lian, X. Wu, E. K. L. Yeow, M. H. Jhon, Y. Chan, *ACS Nano* **2014**, 8, 9349.
- [21] S. Kaniyankandy, S. Rawalekar, S. Verma, H. N. Ghosh, *J. Phys. Chem. C* **2011**, 115, 1428.
- [22] M. Jones, S. Kumar, S. S. Lo, G. D. Scholes, *J. Phys. Chem. C* **2008**, 112, 5423.
- [23] S. Kumar, M. Jones, S. S. Lo, G. D. Scholes, *Small* **2007**, 3, 1633.
- [24] Y. Liu, C. Zhang, H. Zhang, R. Wang, Z. Hua, X. Wang, J. Zhang, M. Xiao, *Adv. Mater.* **2013**, 25, 4397.
- [25] Y. Altintas, B. Liu, P. L. Hernández-Martínez, N. Gheshlaghi, F. Shabani, M. Sharma, L. Wang, H. Sun, E. Mutlugun, H. V. Demir, *Chem. Mater.* **2020**, 32, 7874.
- [26] Y. Wang, Q. Wang, X. Zhan, F. Wang, M. Safdar, J. He, *Nanoscale* **2013**, 5, 8326.
- [27] J. Bang, B. Chon, N. Won, J. Nam, T. Joo, S. Kim, *J. Phys. Chem. C* **2009**, 113, 6320.
- [28] R. Tenne, S. Pedetti, M. Kazes, S. Ithurria, L. Houben, B. Nadal, D. Oron, B. Dubertret, *Phys. Chem. Chem. Phys.* **2016**, 18, 15295.
- [29] S. S. Lo, Y. Khan, M. Jones, G. D. Scholes, *J. Chem. Phys.* **2009**, 131, 084714.
- [30] H. Laheld, *Phys. Rev. B* **1995**, 52, 2697.
- [31] M. Dufour, V. Steinmetz, E. Izquierdo, T. Pons, N. Lequeux, E. Lhuillier, L. Legrand, M. Chamarro, T. Barisien, S. Ithurria, *J. Phys. Chem. C* **2017**, 121, 24816.
- [32] F. Shabani, H. D. Baruj, I. Yurdakul, S. Delikanli, N. Gheshlaghi, F. Isik, B. Liu, Y. Altintas, B. Canimkurbey, H. V. Demir, *Small* **2022**, 18, 2106115.
- [33] S. Hu, F. Shabani, B. Liu, L. Zhang, M. Guo, G. Lu, Z. Zhou, J. Wang, J. C. Huang, Y. Min, Q. Xue, H. V. Demir, C. Liu, *ACS Nano* **2022**, 16, 10840.
- [34] S. Ithurria, M. D. Tessier, B. Mahler, R. P. S. M. Lobo, B. Dubertret, A. L. Efros, *Nat. Mater.* **2011**, 10, 936.
- [35] R. Pandya, R. Y. S. Chen, A. Cheminal, M. Dufour, J. M. Richter, T. H. Thomas, S. Ahmed, A. Sadhanala, E. P. Booker, G. Divitini, F. Deschler, N. C. Greenham, S. Ithurria, A. Rao, *J. Am. Chem. Soc.* **2018**, 140, 14097.
- [36] N. N. Schlenskaya, Y. Yao, T. Mano, T. Kuroda, A. V. Garshev, V. F. Kozlovskii, A. M. Gaskov, R. B. Vasiliev, K. Sakoda, *Chem. Mater.* **2017**, 29, 579.
- [37] R. E. Bailey, S. Nie, *J. Am. Chem. Soc.* **2003**, 125, 7100.
- [38] J. E. Bernard, A. Zunger, *Phys. Rev. B* **1986**, 34, 5992.
- [39] B. I. MacDonald, A. Martucci, S. Rubanov, S. E. Watkins, P. Mulvaney, J. J. Jasieniak, *ACS Nano* **2012**, 6, 5995.
- [40] C. S. Schnohr, *Appl. Phys. Rev.* **2015**, 2, 031304.
- [41] P. P. Ingole, G. B. Markad, D. Saraf, L. Tatikondewar, O. Nene, A. Kshirsagar, S. K. Haram, *J. Phys. Chem. C* **2013**, 117, 7376.
- [42] Y. Kelestemur, B. Guzelturk, O. Erdem, M. Olutas, T. Erdem, C. F. Usanmaz, K. Gungor, H. V. Demir, *J. Phys. Chem. C* **2017**, 121, 4650.
- [43] J. Luo, J. Luo, Z. Zheng, Z. Zheng, S. Yan, M. Morgan, X. Zu, X. Xiang, W. Zhou, *ACS Photonics* **2020**, 7, 1461.
- [44] S. C. Rai, K. Wang, J. Chen, J. K. Marmon, M. Bhatt, S. Wozny, Y. Zhang, W. Zhou, *Adv. Electron. Mater.* **2015**, 1, 1400050.
- [45] K. Wu, Q. Li, Y. Jia, J. R. McBride, Z. X. Xie, T. Lian, *ACS Nano* **2015**, 9, 961.
- [46] S. H. Wei, S. B. Zhang, A. Zunger, *J. Appl. Phys.* **2000**, 87, 1304.
- [47] Y. Kelestemur, M. Olutas, S. Delikanli, B. Guzelturk, M. Z. Akgul, H. V. Demir, *J. Phys. Chem. C* **2015**, 119, 2177.
- [48] T. Watanabe, K. Takahashi, K. Shimura, D. Kim, *Phys. Rev. B* **2017**, 96, 035305.
- [49] B. Pejova, B. Abay, I. Bineva, *J. Phys. Chem. C* **2010**, 114, 15280.
- [50] V. Kumar, V. Jha, A. K. Shrivastava, *Cryst. Res. Technol.* **2010**, 45, 920.
- [51] A. V. Rodina, A. L. Efros, *Phys. Rev. B* **2016**, 93, 155427.
- [52] D. Valerini, A. Cretif, M. Lomascolo, L. Manna, R. Cingolani, M. Anni, *Phys. Rev. B: Condens. Matter Mater. Phys.* **2005**, 71, 235409.
- [53] D. Norris, A. L. Efros, M. Rosen, *Phys. Rev. B* **1996**, 53, 16347.
- [54] S. Ithurria, M. D. Tessier, B. Mahler, R. P. S. M. Lobo, B. Dubertret, A. L. Efros, *Nat. Mater.* **2011**, 10, 936.
- [55] P. C. Sercel, A. L. Efros, *Nano Lett.* **2018**, 18, 4061.
- [56] R. Scott, S. Kickhöfel, O. Schoeps, A. Antanovich, A. Prudnikau, A. Chuvilin, U. Woggon, M. Artemyev, A. W. Achtstein, *Phys. Chem. Chem. Phys.* **2016**, 18, 3197.
- [57] R. Winik, D. Cogan, Y. Don, I. Schwartz, L. Gantz, E. R. Schmidgall, N. Livneh, R. Rapaport, E. Buks, D. Gershoni, *Phys. Rev. B* **2017**, 95, 235435.
- [58] H. H. Fang, J. Yang, S. Adjokatse, E. Tekelburg, M. E. Kamminga, H. Duim, J. Ye, G. R. Blake, J. Even, M. A. Loi, *Adv. Funct. Mater.* **2020**, 30, 1907979.
- [59] A. G. D. Águila, E. Groeneveld, J. C. Maan, C. De Mello Donegá, P. C. M. Christianen, *ACS Nano* **2016**, 10, 4102.
- [60] R. Pandya, V. Steinmetz, Y. Puttisong, M. Dufour, W. M. Chen, R. Y. S. Chen, T. Barisien, A. Sharma, G. Lakhwani, A. Mitoglu, P. C. M. Christianen, L. Legrand, F. Bernardot, C. Testelin, A. W. Chin, S. Ithurria, M. Chamarro, A. Rao, *ACS Nano* **2019**, 13, 10140.
- [61] Z. Deutsch, L. Neeman, D. Oron, *Nat. Nanotechnol.* **2013**, 8, 649.
- [62] G. Yang, M. Kazes, D. Raanan, D. Oron, *ACS Photonics* **2021**, 8, 1909.
- [63] M. H. Humayun, P. L. Hernandez-Martinez, N. Gheshlaghi, O. Erdem, Y. Altintas, F. Shabani, H. V. Demir, *Small* **2021**, 17, 2103524.
- [64] G. Xing, Y. Liao, X. Wu, S. Chakraborty, X. Liu, E. K. L. Yeow, Y. Chan, T. C. Sum, *ACS Nano* **2012**, 6, 10835.
- [65] M. Olutas, B. Guzelturk, Y. Kelestemur, A. Yeltik, S. Delikanli, H. V. Demir, *ACS Nano* **2015**, 9, 5041.
- [66] R. Scott, A. W. Achtstein, A. Prudnikau, A. Antanovich, S. Christodoulou, I. Moreels, M. Artemyev, U. Woggon, *Nano Lett.* **2015**, 15, 4985.